Short title: Probing leaf plastid volumes in situ

Correspondence:

Hans-Henning Kunz

Department for Plant Biochemistry LMU Munich,

Großhadernerstr. 2-4,

82152 Planegg-Martinsried, Germany

Email: kunz@lmu.de

Probing the *in-situ* volumes of Arabidopsis leaf plastids using 3D confocal and scanning electron microscopy.

Jan Knoblauch[a], Rainer Waadt[c], Asaph B. Cousins[a], Hans-Henning Kunz[a,b]*

[a] School of Biological Sciences, Washington State University, PO Box 644236, Pullman, WA 99164-4236, USA

[b] LMU Munich, Plant Biochemistry, Großhadernerstr. 2-4, 82152 Planegg-Martinsried, Germany

[c] Institute of Plant Biology and Biotechnology, University of Münster, Schlossplatz 7, 48149 Münster, Germany

*Corresponding author: Hans-Henning Kunz, kunz@lmu.de

The author responsible for distribution of materials integral to the findings presented in this article in accordance with the policy described in the Instructions for Authors (https://academic.oup.com/plphys/pages/General-Instructions) is Hans-Henning Kunz.

Keywords:

One-sentence summary

This work describes and compares three different strategies to obtain accurate volumes of leaf plastids from Arabidopsis, the most widely used model plant.

Footnotes:

Author Contributions

- H.-H.K. designed research. J.K. performed most experiments and analyzed data. R.W. designed and cloned the envelope fluorescence marker construct. A.B.C. analyzed and discussed data. All authors wrote and assisted in editing the manuscript.

Funding

- J.K.'s work was funded by an NSF Career Award (IOS-1553506) and a third call ERA-CAPS grant from NSF (IOS-1847382) to H.-H.K. R.W. received funding from the Deutsche

Forschungsgemeinschaft (DFG; WA 3768/4-1). H.-H.K. is funded by the Deutsche Forschungsgemeinschaft (DFG) (SFB-TR 175, project B09).

Abstract

Leaf plastids harbor a plethora of biochemical reactions including photosynthesis, the most important pathway on earth. Scientists are eager to unveil the physiological processes within the organelle but also their interconnection with the rest of the plant cell. An increasingly important feature of this venture is to use experimental data in the design of metabolic models. A remaining obstacle has been the limited in situ volume information of plastids and other cell organelles. To fill this gap for chloroplasts, we established three microscopy protocols delivering *in situ* volumes based on: 1) chlorophyll florescence emerging from the thylakoid membrane, 2) a CFP marker embedded in the envelope, and 3) calculations from serial block-face scanning electron microscopy (SBFSEM). The obtained data were corroborated by comparing wild-type data with two mutant lines affected in the plastid division machinery known to produce small and large mesophyll chloroplasts, respectively. Furthermore, we also determined the volume of the much smaller guard cell plastids. Interestingly, their volume is not governed by the same components of the division machinery which defines mesophyll plastid size. Based on our three approaches the average volume of a mature Col-0 wild-type mesophyll chloroplasts is 93 μm^3. Wild-type guard cell plastids are approximately 18 μm^3. Lastly, our comparative analysis shows that the chlorophyll florescence analysis can accurately determine chloroplast volumes, providing an important tool to research groups without access to transgenic marker lines expressing genetically encoded fluorescence proteins or high-end costly SBFSEM equipment.

58 **Introduction**

59 Photosynthesis, the light-driven CO_2 fixating pathway, is the foundation of life and global food
60 production. In land plants, this pathway is housed in the chloroplast, a specialized plastid-type of
61 endosymbiotic origin located in mesophyll or bundle sheath leaf cells. Chloroplasts are only one
62 of several plastid-types found in the various diverse plant tissues (Choi et al., 2021), with the
63 proplastid representing the most basic undifferentiated precursor organelle (Jarvis and López-Juez,
64 2013). Through highly coordinated gene expression involving the nuclear and the organellar
65 genome, proplastids develop into chloroplasts, amyloplasts, chromoplasts etc., all with distinct
66 morphologies and varying sizes (Liebers et al., 2017; Sun et al., 2017). Depending on plant age
67 some plastid types can interconvert (Jarvis and López-Juez, 2013). The number of plastids can
68 surpass 100 per cell in *Arabidopsis thaliana*, contributing to about a quarter of the total cell volume
69 (Crumpton-Taylor et al., 2012; Unal et al., 2020). The abundance of genetically identical plastids
70 occurs through binary fission facilitated by a complex contractile FtsZ ring inside the organelle
71 and additional plastid-dividing (PD) rings that contain proteins anchored or associated with the
72 inner and outer envelope membrane (Yoshida, 2018; Osteryoung and Pyke, 2014; Chen et al.,
73 2018). The discovery of this intricate machinery was investigated through several loss and gain-
74 of-function mutants of FtsZ and PD ring components. These mutants represent invaluable research
75 tools to understanding both organelle fission and the significance of plastid abundance and size on
76 basic physiological responses such as light stress avoidance (Dutta et al., 2017).

77 Plastids carry out general and highly specialized biochemical reactions, many yielding
78 phytohormones or their respective precursors, which are critical for plant development and stress
79 response (Bittner et al., 2022). Unsurprisingly, understanding plastid and chloroplast function has
80 been the focus of many scientists interested in a wide range of topics, from photosynthesis to the

81 importance of plastids for plant environmental interactions (Kleine et al., 2021). In recent years,
82 computational modeling of energy/metabolic flux has given new insights into the complex inner
83 workings of the organelle (Krantz et al., 2021; Fürtauer et al., 2018). This modeling has been added
84 by non-aqueous fractionation to determine how these organelles interact (Klie et al., 2011;
85 Fürtauer et al., 2016; Höhner et al., 2021). Nevertheless, the efficacy of these models would be
86 further improved with precise determination of organellar volumes. This is especially important
87 for *A. thaliana*, arguably the most studied plant worldwide and the primary model plant system for
88 elucidating the molecular, structural, and biochemical control of energy/metabolic fluxes
89 (Woodward and Bartel, 2018).

90 Chloroplast dimensions and volumes are most often inferred using two-dimensional (2D)
91 imaging techniques (Kunz et al., 2014; Aranda-Sicilia et al., 2016; Unal et al., 2020). Transmission
92 electron microscopy (TEM) has been the primary method for obtaining these 2D images. However,
93 TEM requires fixation which can result in tissue, cellular, and organellar shrinkage. For instance,
94 spinach chloroplasts loose about 30% of their volume during the fixation procedure (Winter et al.,
95 1994). Also, TEM imaging is error-prone since optimal imaging quality requires 60-80 nm thick
96 sections and it is impossible to know what plane of the chloroplast is visible or the angle of the
97 section. This means it is unclear if a given chloroplast image is a glancing section or cuts through
98 the center, making accurate volume calculations challenging with a bias towards underestimating
99 volumes. This uncertainty leads to considerable variation in estimated chloroplast volumes and
100 requires large time-consuming datasets to approximate accurate chloroplast volumes even within
101 a single cell. A recent study using wheat and chickpea demonstrated that the 2D approach of
102 estimating chloroplast volumes is inaccurate and prone to volume underestimations (Harwood et
103 al., 2019).

104 The recent application of technologies to create three-dimensional (3D) representations of
105 leaf anatomy, including the serial block-face scanning electron microscopy (SBFSEM), has
106 introduced alternative ways to address ongoing uncertainty in chloroplast volumes (Denk and
107 Horstmann, 2004). In short, SBFSEM employs automated collection of serial surface images from
108 a resin-embedded sample block. This occurs via an internal ultramicrotome that cuts a 40-80 nm
109 thin section. The newly exposed surface of the truncated sample block is scanned to generate the
110 next SEM image. However, the SBFSEM technology requires significant specialized
111 instrumentation, and similar with TEM has potential difficulties with sample fixation and
112 preparation that may result in inferior images and data misinterpretation.

113 Live imaging of leaf tissue using confocal microscopy can avoid the errors associated with
114 fixation, such as chloroplast shrinkage. Confocal microscopy does, however, present its own
115 challenges and limitations. While there is no risk of chloroplast deformation due to fixation, the
116 relatively long wavelength of light drastically lowers the achievable imaging resolution compared
117 to electron microscopy. Additionally, since most confocal microscopes utilize a pinhole to image
118 optical sections inside the sample tissue, the fluorescence is scattered by the tissue it passes through
119 before reaching the objective, lowering resolution and limiting the depth accurate imaging can be
120 done to. As long as this is taken into consideration, however, confocal can be powerful tool as it
121 also allows for colocalizing several fluorophores within the sample, allowing for easy visualization
122 of one or more structures of interest.

123 In this study, we use three different 3D imaging techniques to measure leaf chloroplast
124 volumes in *A. thaliana* (Figure 1A). Two protocols employ confocal microscopy z-stacks using
125 chlorophyll fluorescence or a chloroplast envelope marker, respectively, as easy to replicate, more
126 accessible methods. The third approach is based on SBFSEM and 3D reconstruction. To validate

127 our assays, we used three different *A. thaliana* genotypes: 1) Col-0 as a wild-type control, 2) *35s-*
128 *PDV1 35s-PDV2*, which has more, smaller chloroplasts, and 3) *arc5-2*, having fewer but gigantic
129 chloroplasts per cell (Osteryoung, 2017). The *35s-PDV1 35s-PDV2* and *arc5-2* are chloroplast
130 division mutants and were chosen to quantify the accuracy of each volume determination
131 approach.

132 **Results & Discussion**

133 **Mesophyll chloroplast volume measurements using chlorophyll fluorescence**

134 For plastid volume calculations three different, wild type and previously described genotypes were
135 selected. *35s-PDV1 35s-PDV2* has smaller chloroplasts caused by the overexpression of the outer
136 envelope PLASTID DIVISION1 (*PDV1*) and PLASTID DIVISION2 (*PDV2*) proteins, which
137 recruit the ARC5/DRB5P ring during chloroplast division (Okazaki et al., 2009; Dutta et al., 2017).
138 Conversely, *arc5-2* is a T-DNA insertion loss of function mutant that exhibits a low number of
139 gigantic chloroplasts per cell. The *ARC5* locus encodes one of the outer envelope membrane
140 proteins responsible for assembling the most outer PD ring (Robertson et al., 1996; Miyagishima
141 et al., 2006). Col-0 was used as a wildtype control. All genotypes exhibited a similar green leaf
142 color and were indistinguishable from controls with regards to their growth rate and appearance
143 (Figure 1B). The reported chloroplast phenotypes became visible in the micrographs (Figure 1C-
144 D). For all experiments, leaf discs were collected from the first three mature true leaves. Three
145 separate grow-outs per genotype were utilized to test the consistency of our results. Initially,
146 chloroplast volumes were calculated based on confocal microscopy z-stacks of chlorophyll
147 fluorescence (supplemental movies 1-3), which emerges from the thylakoid membrane (Figure
148 1E). Across all three grow-outs, Col-0 mesophyll chloroplasts had an average volume of 88.24 ±
149 1.58 μm^3. *35s-PDV1 35s-PDV2* showed a clear trend towards slightly smaller mesophyll

150 chloroplast volumes with an average volume of 60.13 ± 1.05 μm^3. Lastly, *arc5-2* chloroplast
151 volumes were significantly greater (one-way ANOVA, $p<0.05$) as in wild-type and *35s-PDV1 35s-*
152 PDV2 plants, averaging at 1538 ± 145 μm^3. Frequency distribution plots of the combined volume
153 data collected on all three genotypes are shown in Supplemental Figure 1A-B. Comparing different
154 grow-outs, minor differences in chloroplast volumes can be observed within each genotype. For
155 all three genotypes, the second grow-out season gave rise to slightly lower average chloroplast
156 volumes than the first and third season indicating minor seasonal effects. However, statistical
157 analysis within each genotype did not indicate significant differences between grow-outs (one-
158 way ANOVA, $p<0.05$).

159 On average, Col-0 contained 74 ± 3 chloroplasts per mesophyll cell (Figure 1F). This is in
160 the middle range compared to reports by others suggesting averages of 60, 76 (± 5) or between 80
161 and 120 chloroplasts per cell (Kinsman and Pyke, 1998; Okazaki et al., 2009; Crumpton-Taylor et
162 al., 2012). In line with the literature, *35s-PDV1 35s-PDV2* and *arc5-2* mesophyll cells contained
163 on average 92 ± 5 and 5 ± 0.5 chloroplasts, respectively (Miyagishima et al., 2006; Okazaki et al.,
164 2009). The differences between studies can be related to different mesophyll cell types,
165 developmental states, or to local growth conditions which were all reported to affect plastid
166 numbers (Antal et al., 2013).

167 **Guard cell plastid volume measurements using chlorophyll fluorescence**

168 Guard cell chloroplasts are known to be smaller than mesophyll chloroplasts (Pyke and Leech,
169 1994). Thus, we also assayed guard cell plastid volumes to test the feasibility of our protocol across
170 different cell types. When comparing guard cell chloroplast volumes, no differences between
171 genotypes were observed. For Col-0 chloroplast volumes averaged at 17.69 ± 0.21 μm^3, while
172 volumes for *35s-PDV1 35s-PDV2*, and *arc5-2* were 18.04 ± 0.26 μm^3, and 17.26 ± 0.28 μm^3

173 respectively (Figure 1G). Comparing the genotypes by one-way ANOVA showed no statistically
174 significant difference ($p<0.05$). Supplemental figure 2 shows an overlapping frequency
175 distribution for the three genotypes' guard cell plastid volumes. When comparing the three grow-
176 outs individually the same pattern can be seen. In summary, our data are in line with previous
177 reports on *arc5* mutants showing that loss of *ARC5* affects mesophyll but not guard plastid sizes
178 (Pyke and Leech, 1994).

179 As shown above, guard cell chloroplast volumes are similar between Col-0 and the two
180 mutants affected in mesophyll chloroplast division. Similarly, the number of plastids per guard
181 cell was not significantly different (Figure 1H): Col-0 guard cells contained 4.5 ± 1.0 chloroplasts
182 on average, which aligns with previous research done on this (Fujiwara et al., 2019), while both
183 *35s-PDV1 35s-PDV2* and *arc5-2* contained only 3.6 ± 0.83 chloroplasts on average. Some
184 previous studies reported immature, non-fluorescing plastids in *arc5-2* guard cells (Fujiwara et al.,
185 2018). Since no brightfield images were acquired in this study, we cannot comment on this
186 observation as we only visualized fluorescing plastids. Also, giant chloroplasts were previously
187 found in rare instances in *arc5*-2 guard cells (Fujiwara et al., 2018), which we did not encounter.

188 **Mesophyll chloroplast volume measurements using a plastid outer envelope fluorescence**
189 **marker protein**

190 Chlorophyll fluorescence emerges from the thylakoid membrane pigments and thus may not
191 effectively represent the entire volume of the chloroplast. Therefore, a cyan-fluorescence protein
192 (CFP) envelope marker localized to the outer chloroplast envelope was employed. Initially, a Col-
193 0 wild-type line with robust CFP signal was isolated using confocal microscopy (Figure 2A-C).
194 Since strong overexpression of envelope proteins can result in membrane alterations, we ensured
195 that this did not occur in the lines selected for this study (Breuers et al., 2012). Subsequently, the

196 marker gene was introgressed into the *35s-PDV1 35s-PDV2* and *arc5-2* mutants with known
197 plastid volume differences. Once homozygous F3 plants were available, we acquired z-stacks of
198 both, the envelope CFP marker and chlorophyll fluorescence signals in parallel from all three
199 genotypes. As expected, average chloroplast volumes calculated using the envelope marker was
200 slightly higher than that calculated using chlorophyll fluorescence (Figure 2D). For Col-0 the
201 average volume for chlorophyll fluorescence and the envelope marker were 78.9 $\mu m^3 \pm 2.6$ and
202 94.7 ± 2.9 μm^3 respectively, for *35s-PDV1 35s-PDV2* they were 55.6 $\mu m^3 \pm 2.4$ and 63.1 ± 2.0
203 μm^3 respectively, and for *arc5-2* the values were 1714.9 $\mu m^3 \pm 222.7$ and 2232.0 ± 330.0 μm^3,
204 respectively. Statistical analyses comparing chlorophyll fluorescence and envelope marker
205 volumes within each genotype, did not show a significant difference in values ($p<0.05$), albeit a
206 trend was clear. When comparing different genotypes, the same observation emerged i.e.,
207 statistically significant higher volumes exist only between *arc5-2* and the two other lines. Col-0
208 volumes based on chlorophyll fluorescence reflect to the lower end found in the three, independent
209 grow-out experiment previously (Figure 1G). Seasonal effects are the most likely explanation.

210 **Chloroplast volume determination using serial block-face scanning electron microscopy**

211 When it comes to the application in plant tissues, serial block-face scanning electron microscopy
212 (SBFSEM) is still a relatively new imaging technique. In fact, for *A. thaliana* mesophyll cell
213 organelles there are no published volume data yet. Thus, we performed SBFSEM as an orthogonal,
214 more high-resolution method for chloroplast analysis. Imaging was done for the same three
215 genotypes as described above. Since the tissue has to be fixed, dehydrated and embedded, osmotic
216 alterations may have an influence on organelle volume. The protocol used here and described in
217 the materials and methods section was developed as part of a study to improve SBFSEM protocols
218 and analysis in plant tissues (Mullendore et al. in preparation). This includes a machine learning

219 algorithm "ANATOMICS MLT" which was used for this study to auto-label large image data sets.
220 Figure 3A shows chloroplasts labeled by ANATOMICS MLT. The average chloroplast volume
221 determined for Col-0 was 92.9 ± 1.3 μm^3. For *35s-PDV1 35s-PDV2*, and *arc5-2* the volumes were
222 69.4 ± 0.8 μm^3, and 1970 ± 759 μm^3, respectively (Figure 3B-C). As for all previous imaging
223 techniques used, only trends in chloroplast volumes difference could be identified between *35s-*
224 *PDV1 35s-PDV2* and Col-0, while both genotypes were significantly different from *arc5-2*. A full
225 image stack reconstruction for each genotype can be found as supplemental movies 4-6.

226 **Protocol comparisons and recommendations**

227 In this study, we set out to gather accurate volume information from mesophyll and guard cell
228 plastids of the model plant *A. thaliana*. In addition, we wanted to test the feasibility of employing
229 standard confocal microscopy, available in most biology departments, to determine organellar
230 volumes. When comparing between imaging approaches, chloroplast volumes were relatively
231 consistent (about 93 μm^3 in wild-type plants), with volumes derived by an outer envelope marker
232 protein showing a slightly higher average between 10-20% when compared to both chlorophyll
233 fluorescence and SBFSEM measurements (Figure 4A-C, Supplemental Table 1). However, when
234 running a one-way ANOVA comparing chloroplast volumes measured by each of the three
235 imaging techniques, no statistically significant difference ($p<0.05$) was found within either of the
236 genotypes, regardless of the imaging approach applied. Slightly higher average volumes using data
237 from the envelope marker are to be expected, as it defines the outer boundary of a chloroplast and
238 thus encompasses envelope membranes, inter membrane space, and the stroma. In contrast,
239 chlorophyll fluorescence primarily represents the volume determined by thylakoid membranes.
240 One limitation we observed when subtracting the chlorophyll fluorescence from the outer
241 envelope-based volume is that the obtained values are too low (≈ 16 μm^3) to accurately reflect the

242 stromal volume. According to the literature the stroma is expected to occupy about 50% of a plastid
243 (Antal et al., 2013). This shortcoming can be explained by the insufficient resolution of confocal
244 micrographs which does not allow to accurately resolve the stroma between thylakoid membranes.

245 The critical advantage of SBFSEM is the much higher resolution compared to confocal or
246 super-resolution microscopy, but much faster acquisition time than focused ion beam
247 methodologies. Therefore, it allows to image large tissue areas with hundreds or thousands of cells
248 within reasonable time (days) while allowing to acquire surface areas and volumes of organelles
249 that are too small to image by light microscopy-based methods (e.g., confocal) such as the ER or
250 Golgi apparatus. It is however critical that appropriate protocols are used to maintain the volume
251 of organelles. Chloroplasts are large enough to serve as a tool to compare volumes taken by
252 confocal microscopy and SBFSEM. It is reasonable to assume that if chloroplast volumes between
253 in situ and embedded tissue are similar, other organelle volumes in the embedded tissue will be
254 accurate as well.

255 The difference in chloroplast volumes between chlorophyll fluorescence and SBFSEM
256 images is surprisingly small and not statistically significant, showing that our protocol provides
257 excellent maintenance of the tissue. All chloroplasts in our SBFSEM micrographs appear intact
258 (no sharp edges which are usually an indication of shrinkage) and undamaged. Nevertheless,
259 fixative and buffers concentrations as well as the dehydration procedure may have to be tailored
260 to other specimen types such as stems and roots or other plant species. Stains can also be adjusted
261 to fit organelles or structures of interest. Usually this requires a fair amount of strategic trial and
262 error. However, SBFSEM currently allows standard resolutions of down the 10 nm at comparably
263 high acquisition speeds which is a massive improvement over other available technology. As we

264 show in this study, accurate quantitative anatomical data comparable to in situ studies can be
265 achieved.

266 The chloroplast division mutants used as a proof of concept in this study demonstrates the
267 ability and limitations to quantify volume differences. While each method confirmed the drastic
268 mesophyll plastid size variation between Col-0 and *arc5-2* plants, the expectedly smaller
269 differences between Col-0 and *35s-PDV1 35s-PDV2* were only revealed by trend but not with
270 sufficient statical power to allow strong conclusions regardless of the imaging applied. Volume
271 differences between mesophyll and guard cell chloroplasts were also successfully resolved.
272 Interestingly, while mesophyll chloroplast volumes varied among genotypes, guard cell plastids
273 had consistent volumes and numbers throughout. This provides more evidence that guard cell and
274 mesophyll plastid division are governed by distinct genetic programs.

275 When comparing our results with the literature we find quite stark differences. While we
276 determined the Col-0 wild-type mesophyll chloroplast using orthogonal approaches at a size of ≈
277 93 μm^3 most publications refer to old volume studies on other species and an average value of ≈
278 31 μm^3 (Antal et al., 2013; Nobel, 2020). Although mesophyll chloroplast sizes seem highly
279 species- and to a minor degree daytime-dependent the values from spinach, pea, tobacco, wheat,
280 poplar are in the range from 15 to 35 μm^3 and appear to be rather underestimations (Antal et al.,
281 2013; Nobel, 2020). At least side by side in a light microscope *A. thaliana* and pea chloroplast do
282 not seem to drastically differ in size (Schulz et al., 2004). Recent 3D assays describe wheat
283 chloroplasts at 114.6 ± 21.5, chickpea at 22.4 ± 10.2 μm^3, and rice at 47 μm^3 (Oi et al., 2017;
284 Harwood et al., 2020). For *A. thaliana* only one study on cotyledon development was found to
285 report 3D derived plastid volume data (Pipitone et al., 2021). Albeit only three plastids were
286 assayed by SBF-SEM the obtained value of 112.14 μm^3 (±4.3) is roughly in the same range as the

287 93 μm^3 we recorded from mesophyll chloroplasts in mature true leaves. In conjunction, both
288 studies emphasize that *A. thaliana* chloroplasts are far bigger than the often-suggested average
289 plastid volume of 31 μm^3. This needs to be taken into account when organelle volumes are
290 employed in flux models. Additionally, because of the wide range of plastids sizes reported from
291 different species generalizing metabolic flux assumptions can be problematic. Fortunately, as we
292 show through our study rapid z-stack recordings based on chlorophyll fluorescence using a
293 standard confocal microscope gives sufficiently accurate volume information to survey this data
294 point for any given plant species of interest. Since we obtained very similar values regardless of
295 the approach employed, we can state with high confidence that a volume of $\approx$ 93 μm^3 reflects the
296 natural in situ situation in the model plant Arabidopsis. Moreover, the fixation-staining protocol
297 we utilized for SBFSEM is well-suited for plastids. The low deviation from values obtained via
298 fixation-staining-free confocal microscopy confirms that no shrinkage occurred in our specimens.

299 **Conclusions**

300 Overall, comparing chloroplast volumes from plastid division mutants acquired through different
301 imaging methods shows relatively close overlap of volumes. This suggests that even though z-
302 stack confocal micrographs have much lower resolution than SBFSEM, they still give fairly
303 accurate volume data. Between the two confocal microscopy methods, using an envelope marker
304 will yield more accurate total chloroplast volumes. Nevertheless, for a much easier and faster
305 estimation, chlorophyll fluorescence delivers high replicate numbers and is thus quite accurate.
306 Moreover, it does not require cloning, transformation or introgression of a fluorescence protein
307 encoding transgene. SBFSEM yields the most accurate volume data due to its much higher
308 resolution. However, lengthy sample preparation procedure optimization might be necessary to
309 prevent artifacts resulting in skewed volumes. Researchers are advised to consider our conclusions

310 for balanced and informed decision-making which answer the question at hand with the best
311 equipment available to them.

312 **Materials and Methods**

313 **Plant Material**

314 *A. thaliana* plants used: Columbia-0 as a control, *arc5-2* (SAIL_71_D11), a giant chloroplast
315 mutant due to a knockout of the *ARC5* chloroplast division gene, and 35*S-PDV1 35S-PDV2* with
316 smaller chloroplasts caused by overexpression of *PDV1* and *PDV2* (Miyagishima et al., 2006;
317 Okazaki et al., 2009; Dutta et al., 2017). These plants were grown in a Conviron growth chamber
318 (Winnipeg, Man, Canada) using a 16/8-hour light/dark cycle at 150 µmol photons $m^{-2}s^{-1}$,
319 21°C/19°C day/night cycle and 60-80% humidity on soil. Approximately, 100 seeds per genotype
320 were sown into one 1.15-quart pot with soil (Sungro Professional Growing Mix #1, Sun Gro
321 Horticulture, Agawam, MA, USA), and after a week, the ten largest seedlings were transferred
322 into individual 0.59-pint pots and grown for 4 additional weeks before imaging.

323 To target a fluorescent marker to the outer chloroplast envelope surface, the coding sequence (192
324 bp) of the outer envelope protein 7.1 (OEP7; At3g52420) without its Stop codon and with a Gly-
325 Gly-Ser-Gly-linker at the 3'-end was first amplified using Q5 High-Fidelity DNA Polymerase
326 (New England Biolabs) and the primers GGB_OEP7_F –
327 AACAGGTCTCAAACAATGGGAAAAACTTCGGGAGC and GGC_OEP7_GGSG_R –
328 AACAGGTCTCTAGCCTCCAGATCCTCCCAAACCCTCTTTGGATGTGG, followed by
329 FastDigest Eco31I (Thermo Fisher Scientific) digestion, and ligation into the GreenGate module
330 backbone pGGB (Lamproupolos et al., 2013). Together with previously described GreenGate
331 modules (Lamproupolos et al., 2013; Waadt et al., 2017), OEP7, the orange fluorescing

332 mNectarine (Johnson et al., 2009) without Start codon, and the cyan fluorescing mTurquoise
333 (Goedhart et al., 2010) with a 5'-end Gly-Ser-linker were ligated into the plant expression vector
334 pGGZ003 yielding the plasmid pGGZ-RW105 (pGGZ003-pUBQ10-OEP7-GGSG-
335 mNectarine_ATG-GSL-mTurquoise-tHSP18.2M-hygR). This construct was then transformed
336 into Col-0 wild-type by floral dip, and positive transformants were selected through germination
337 on hygromycin (15 µg ml^{-1}, Chem-Impex, Wood Dale, IL, USA). Subsequently, the envelope
338 marker was introgressed into *arc5-2* and *35s-PDV1 35s-PDV2* mutant lines.

339 **Confocal Laser Scanning Microscopy**

340 **Mesophyll Chloroplast Fluorescence Volume Measurements**

341 For mesophyll imaging, fresh leaf disks of 1 cm diameter were taken from the center of a mature
342 leaf and imaged with a HC PL APO CS2 63x/1.20 NA water-immersion objective on a Leica SP8
343 confocal laser-scanning microscope (Leica Biosystems, Deer Park, IL, USA). Chlorophyll was
344 excited using a 405 nm pulsed laser and the fluorescence was collected using a HyD detector set
345 to 650-720 nm. The gain was optimized for each stack, using the brightness indicator. Additional
346 imaging parameters were: scanning speed 100 Hz, zoom 2, line average 2, pinhole 1, and z-stacks
347 system optimized with 0.305-µm-thick optical sections for volume analysis. Number of z-sections
348 varied, and stacks were later cropped to exclude images where the fluorescence border could not
349 be accurately identified.

350 **Guard Cell Chloroplast Volume Measurements**

351 For imaging of guard cell chloroplasts, the abaxial side of the leaf was used as there are more
352 stomata present. The abaxial side of a leaf was glued to a glass slide using medical adhesive
353 (Hollister, Libertyville, IL, USA). After allowing the glue to dry, leaf tissue was removed by

354 scraping with a razor blade until the lower epidermis became exposed (Azoulay-Shemer et al.,
355 2016). Guard cells turgescence was determined visually and used to checked for intactness, and
356 guard cell chloroplasts were then imaged using a HC PL APO CS2 63x/1.40 oil-immersion
357 objective. Z-stacks were taken using 0.255-µm-thick optical sections. Otherwise, images were
358 taken as described above.

359 **mTurquoise Imaging**

360 Plants with chloroplast envelopes tagged with mTurquoise were also imaged using a HC PL APO
361 CS2 63x/1.20 NA water-immersion objective on a Leica SP8 confocal laser-scanning microscope
362 (Leica Biosystems, Deer Park, IL, US). Dual channels were used to image mTurquoise
363 simultaneously with chlorophyll fluorescence. A HyD detector set to 460-520 was used to collect
364 mTurquoise fluorescence, while a HyD detector set to 650-720 nm was used for chlorophyll
365 fluorescence. All other imaging parameters were as described above.

366 **Chloroplast Volume Analysis**

367 Chloroplast reconstruction and analysis was done using ImageJ software, utilizing the Bio-Formats
368 plugin to import .lif files (https://github.com/ome/bioformats). After importing a z-stack, and
369 manually thresholding to optimize chloroplast outlines, a Median Filter (Radius: 2.0) was applied
370 for smoothing and subtract (~10), a global brightness reduction tool, was used to remove
371 background noise. Chloroplast volumes were extracted with the 3D Objects Counter function in
372 ImageJ, and the resulting labels were checked to ensure only volumes of complete chloroplasts
373 were counted.

374 **Serial Block Face Scanning Electron Microscopy (SBFSEM)**

375 **Fixation Protocol**

376 Arabidopsis leaves were removed from the plant, cut into 2 mm x 2 mm squares, and put into a
377 fixative solution containing 4% glutaraldehyde, 2 mM $CaCl_2$ in 0.1 M cacodylate buffer (pH 6.8)
378 for 6 hours at room temperature. Samples were then microwaved at 300W at a 35°C maximum
379 temperature limit for 2 min and then washed 3x for 10 minutes in 0.1 M cacodylate buffer followed
380 by a post-fixation with 1.5% KFeCN, 2% OsO_4, 2 mM $CaCl_2$, in 0.15 M cacodylate buffer
381 overnight at 4°C. After washing 3x for 10 min in double distilled water (ddH_2O) at room
382 temperature, samples were incubated in 0.2% gallic acid for 1 hour at room temperature, and then
383 washed 3x for 10 minutes in ddH_2O. A secondary post-fixation was done in 2% OsO_4 for 3 hours
384 at room temperature, and after washing 3x for 10 min in ddH_2O, a 2% uranyl acetate incubation
385 was applied overnight at 4°C. Samples were washed 3x for 10 minutes in ddH_2O at room
386 temperature, then stained with Walton's lead aspartate (Walton, 1979) at 60°C for one hour and
387 finally washed 3 times for 10 min in ddH_20 at room temperature.
388
389 Samples were dehydrated with an acetone series using freshly mixed acetone solutions. 10% steps
390 were done between 10%-50% (v/v) acetone for 10 min at room temperature. A second exchange
391 of 50% acetone was incubated at -20°C for 1 hour. For the remainder of the dehydration series,
392 exchanges were performed at -20°C overnight in 60%, 70% ,80% ,90% ,100% ,100%, 100% (v/v)
393 acetone. After the third 100% acetone treatment, samples were incubated overnight and then
394 moved to room temperature to acclimate for ~30 min before the final dehydration in 100% acetone
395 two times for 10 minutes at room temperature.
396
397 Samples were infiltrated in Spurr's resin (Sigma Aldrich, St. Louis, MO, USA) in 3:1, 2:1, 1:1,
398 1:2, 1:3, 100% acetone:hard Spurr resin without the hardener of the resin (DMAE) to prevent

399 premature polymerization, each overnight at room temperature on a rotator. This was followed by
400 two exchanges of 100% hard Spurr's resin with DMAE, overnight at room temperature on a
401 rotator, with the lids removed. Finally, samples were microwaved at 100W and 40°C for 1 hour
402 and subsequently put into a 70°C oven to polymerize.

403 **Imaging**

404 To prepare samples for SBFSEM, the embedded tissue was trimmed and sectioned using a Leica
405 EM UC7 ultramicrotome. Ultrathin sections (~70 nm) were taken and checked for quality using a
406 FEI Technai G2 20 Twin (Thermo Fisher, Waltham, MA, USA). Samples were then transferred to
407 a SBFSEM stub, which is the sample holder, trimmed on the ultramicrotome using a glass knife,
408 after which a Technics Hummer V Sputter Coater was used to apply 10 nm of gold coating. For
409 imaging, an Apreo VolumeScope SEM (Thermo Fisher, Waltham, MA,USA) with the VS-DBS:
410 LoVac lens-mounted BSED detector was used. Imaging conditions were set to 2 kV accelerating
411 voltage, 50 Pa chamber pressure, a beam current of 0.10 nA, a pixel size of 20 x 20 nm, and a
412 dwell time of 3 µs.

413 **Image Processing**

414 The SBFSEM image stacks were processed for volume analysis using software specifically
415 designed to work with SBFSEM stacks, Amira (Thermo Fisher, Waltham, MA, USA). Partial
416 stacks (~500 images) were imported into Amira, and a gaussian filter (XY, standard deviation 1,
417 1, kernel size factor 2) was used to remove noise. Images are then inverted, resampled (Lanczos
418 Filter, Voxel Size: x= 40, y= 40, z= 40), and then exported as a sequence of 2D tiff files. This
419 process was repeated until the entire SBFSEM stack had been processed and exported as described
420 above. The complete stack of processed images was then imported into Amira, cropped around the
421 area of interest and contrast matched (XY planes, mean & variance) using the best contrasted

image within the stack as a reference. This made the contrast consistent for all images throughout the SBFSEM stack. Auto align slices (Rigid, Align and Resample) was run to automatically align all SBFSEM slices. Images were cropped again to remove overlapping edges created by the alignment, and a median filter (XY planes, 3 iterations, Iterative) was used to remove remaining noise. Finally, the stack was exported as a set of 2D tiff files. The fully processed stack was then imported into ImageJ as an image sequence, manually contrasted, and saved as a tiff, creating a 3D tiff stack.

Volume Analysis

Volume analysis of SBFSEM stacks was done using Anatomics MLT (https://github.com/ajbrookhouse/WSU_PlantBio_ML), a machine learning algorithm designed to analyze volumes, object counts, and surface areas of features within SBFSEM stacks. Amira was used to label all chloroplasts within a sequence of 10 processed images with the Segmentation tool by using the brush, then images and labels were exported as separate 3D tiff files. These stacks were then used in the train function of Anatomics MLT (Training Config: Instance.yaml, 100,000 iterations) to train the program to label chloroplasts. The model was then used in the Auto-Label section to label full image stacks. Finally, the Output Tools tab was designed to analyze data from the created labels and can be used to create mesh or point clouds to visually display the labels. This was used to calculate chloroplast volumes and create Point Clouds of the labels which were viewed and overlayed with original images to check for labeling accuracy using the Visualize tab.

Statistical Analysis

Graphing and statistical analysis was done using GraphPad software (Dotmatics, Boston, MA, USA). Means as well as standard deviation and error were calculated. One-way ANOVAs were used to determine statistical significance between biological replicates, genotypes, and imaging

445 techniques. A 2-way ANOVA was run to analyze volume data within the chloroplast fluorescence
446 dataset, comparing each growth cycle within a genotype to the volumes of chloroplasts between
447 genotypes. A 3-way ANOVA was also used to compare chloroplast volumes of genotypes within
448 each imaging method and to compare volumes of chloroplasts of each genotype between imaging
449 techniques.

450 **Accession numbers**

451 *arc5-2* (SAIL_71_D11, S870785), *35s-PDV1 35s-PDV2, ARC5* (AT3G19720), *PDV1*
452 (AT5G53280), *PDV2* (AT2G16070), *OEP7.1* (At3g52420)

453 **Supplemental Data**

454 Supplemental Figure S1. A, Frequency distribution of all mesophyll chloroplast volumes between
455 *35s-PDV1 35s-PDV2* and Col-0 chloroplast within mesophyll cells show a distribution of *35s-*
456 *PDV1 35s-PDV2* volumes slightly lower than Col-0, not at a statistically significant level. B, a
457 frequency distribution for *arc5-2* shows that volumes below 1000 μm^3 are the most common,
458 however values reach as high as 7000 μm^3.

459 Supplemental Figure S2. Frequency distribution of guard cell chloroplast volumes shows very
460 similar distribution and overall volumes between all three genotypes.

461 Supplemental Table 1: Summary of chloroplast volumes in µm3 calculated using image stacks
462 from each method employed. For each genotype the average and standard error are presented.

463 Supplemental Movie 1-3: Video reconstructions showing confocal Z-stacks of each genotype, *35s-*
464 *PDV1 35s-PDV2*, Col-0 and *arc5-2*, respectively.

465 Supplemental Movie 4: Video reconstruction of scanning through a Col-0 SBFSEM image stack.
466 Chloroplasts are labeled using the machine learning algorithm and displayed in cyan.

467 Supplemental Movie 5: Video reconstruction of scanning through a *35s-PDV1 35s-PDV2*
468 SBFSEM image stack.

469 Supplemental Movie 6: Video reconstruction of scanning through an *arc5-2* SBFSEM image stack.

470 **Acknowledgements**

471 We thank Dr. Katherine W Osteryoung from Michigan State University for providing the original
472 mutant germplasms used in this project. J.K. received the WSU Franceschi training grant to
473 support the microscopy work. J.K. thanks his graduate committee members Drs. Andrew
474 McCubbin and Helmut Kirchhoff (both at WSU) for their support and insights.

475

476 **Figure Legends**

477 **Figure 1: Confocal microscopy reveals changes in gain and loss of function mutants in**
478 **components of the plastid division machinery that are restricted to mesophyll cells. A,** the
479 diagram of the Arabidopsis plant shows the size of the plants when imaging and sample preparation
480 was done. The * indicates the leaves used for imaging, and circles indicate the location on each
481 leaf. From here, these samples were either used immediately for imaging using confocal
482 microscopy or fixed and prepared for SBFSEM. **B**, No apparent changes in plant growth or
483 appearance were observed in long-day cultivated genotypes used in this study, *35s-PDV1 35s-*
484 *PDV2*, Col-0, *arc5-2* (scale bars = 2 cm). **C**, Confocal images of chlorophyll fluorescence for each
485 genotype show clear size differences in mesophyll chloroplasts (scale bars = 25 µm). **D**, Confocal

486 images of guard cell chloroplasts taken using chlorophyll fluorescence shows similar chloroplast
487 volumes within guard cells of the three genotypes investigated (scale bars = 25 µm). **E**,
488 Comparison of mesophyll chloroplast volumes deduced from z-stack of chlorophyll fluorescence
489 recordings. Individual grow-outs are shown for each genotype. Statistical analysis done by one-
490 way ANOVA with Tukey's multiple comparison test ($p<0.05$) showed no significant difference
491 between Col-0 and *35s-PDV1 35s-PDV2* chloroplast volumes, neither in the full dataset, nor
492 between any individual repetitions. Significant differences were observed between *arc5-2* and *35s-*
493 *PDV1 35s-PDV2* but also between *arc5-2* and Col-0 mesophyll chloroplast volumes. Letters above
494 each sample in the graph indicate groups of significance (±SE). **F**, Chloroplast numbers per
495 mesophyll cell were counted and show an inverse relationship to that of chloroplast volumes
496 observed between the genotypes. *35s-PDV1 35s-PDV2* has the highest average number of
497 chloroplasts per cell with around 90 chloroplasts, followed by Col-0 averaging slightly fewer, at
498 around 70 chloroplasts per cell. Finally, *arc5-2* mutants showed by far the lowest chloroplast count
499 per cell with an average of 5 chloroplasts (±SE). **G**, Guard cell chloroplast volumes calculated
500 based on z-stacks of chlorophyll fluorescence recordings, in three separate grow outs, statistical
501 analysis shows no significant difference ($p<0.05$) between any of the genotypes, neither within the
502 whole dataset nor within individual growing cycles. Letters above each data set again show groups
503 of significance (±SE). **H**, Guard cell chloroplast counts show that, unlike the similarities in
504 volumes, a slight difference in average chloroplast number per guard cell can be observed. Col-0
505 guard cells contain on average 4.5 chloroplasts, while both the *35s-PDV1 35s-PDV2* and *arc5-2*
506 genotypes contain only around 3.5 chloroplasts per guard cell (±SE).

507

508 **Figure 2: Comparing mesophyll chloroplast volumes deduced from chlorophyll fluorescence**
509 **and an envelope membrane located fluorescent marker.** Comparison of **A**, chlorophyll
510 fluorescence, **B**, the outer chloroplast envelope labeled with CFP visualized in **C**, as an overlay in
511 Col-0 (scale bar = 10 µm). **D**, comparison between chloroplast volumes extracted by chlorophyll
512 fluorescence and mTurquoise envelope marker shows slightly higher volumes in each genotype
513 when calculated using the mTurquoise marker. A statistically significant difference ($p<0.05$) in
514 chloroplast volumes was only found between Col-0 and *35s-PDV1 35s-PDV2* when compared to
515 *arc5-2* mutants. No significant difference is observed between imaging methods when looking at
516 individual genotypes (±SE).

517

518 **Figure 3: Chloroplast volume analysis using SBFSEM. A**, Reconstructions of Col-0
519 chloroplasts by using SBFSEM. Green objects represent chloroplasts labeled using the machine
520 learning algorithm, while in grey a surface was created by thresholding, representing mostly the
521 cell wall and some other high contrast objects within the cells. **B**, deduced chloroplast volumes
522 measured by SBFSEM imaging. Statistical significance ($p<0.05$) in chloroplast volumes is shown
523 by numbers above each dataset in the graph. A significant difference in chloroplast volumes can
524 only be seen between Col-0 and *arc5-2*, as well as between *35s-PDV1 35s-PDV2*, and *arc5-2*. **C**,
525 A frequency distribution of Col-0 and *35s-PDV1 35s-PDV2* shows a shift in volume distribution
526 between the two genotypes (±SE).

527

528 **Figure 4: Comparison of chloroplast volumes measured by imaging type. A-C**, comparison of
529 mesophyll chloroplast volumes extracted using confocal imaging of chlorophyll fluorescence (Chl

530 *a*), CFP envelope marker, and SBFSEM. The means of the data collected using each imaging
531 method was taken for all genotypes. Each pair of imaging methods is compared by plotting the
532 means (±SE). An identity line was added to highlight differences in means between imaging types
533 in each graph. This shows overall similar volumes and distributions between the methods, with
534 data extracted using the CFP envelope marker showing the largest volumes and chlorophyll
535 fluorescence having the lowest. A one-way ANOVA done for statistical analysis only showing a
536 significant difference ($p<0.05$) when comparing *35s-PDV1 35s-PDV2* and Col-0 volumes acquired
537 by either method to *arc5-2*. No significant difference was found between imaging methods for any
538 genotype.

539

540 **Conflict of interest statement. None declared.**

541 **References**

542 Antal, T. K., Kovalenko, I. B., Rubin, A. B., & Tyystjärvi, E. (2013). Photosynthesis-related
543 quantities for education and modeling. *Photosynthesis Research*, *117*(1–3), 1–30.
544 https://doi.org/10.1007/s11120-013-9945-8

545 Aranda-Sicilia, M. N., Aboukila, A., Armbruster, U., Cagnac, O., Schumann, T., Kunz, H.-H.,
546 Jahns, P., Rodríguez-Rosales, M. P., Sze, H., & Venema, K. (2016). Envelope K^+/H^+
547 Antiporters AtKEA1 and AtKEA2 Function in Plastid Development. *Plant Physiology*, *172*(1),
548 441–449. https://doi.org/10.1104/pp.16.00995

549 Bittner, A., Cieśla, A., Gruden, K., Lukan, T., Mahmud, S., Teige, M., Vothknecht, U. C., &
550 Wurzinger, B. (2022). Organelles and phytohormones: A network of interactions in plant stress

551 responses. *Journal of Experimental Botany*, *73*(21), 7165–7181.
552 https://doi.org/10.1093/jxb/erac384

553 Breuers, F. K. H., Bräutigam, A., Geimer, S., Welzel, U. Y., Stefano, G., Renna, L., Brandizzi,
554 F., & Weber, A. P. M. (2012). Dynamic Remodeling of the Plastid Envelope Membranes – A
555 Tool for Chloroplast Envelope in vivo Localizations. *Frontiers in Plant Science*, *3*.
556 https://doi.org/10.3389/fpls.2012.00007

557 Chen, C., MacCready, J. S., Ducat, D. C., & Osteryoung, K. W. (2018). The Molecular
558 Machinery of Chloroplast Division. *Plant Physiology*, *176*(1), 138–151.
559 https://doi.org/10.1104/pp.17.01272

560 Choi, H., Yi, T., & Ha, S.-H. (2021). Diversity of Plastid Types and Their Interconversions.
561 *Frontiers in Plant Science*, *12*, 692024. https://doi.org/10.3389/fpls.2021.692024

562 Crumpton-Taylor, M., Grandison, S., Png, K. M. Y., Bushby, A. J., & Smith, A. M. (2012).
563 Control of Starch Granule Numbers in Arabidopsis Chloroplasts. *Plant Physiology*, *158*(2),
564 905–916. https://doi.org/10.1104/pp.111.186957

565 Denk, W., & Horstmann, H. (2004). Serial Block-Face Scanning Electron Microscopy to
566 Reconstruct Three-Dimensional Tissue Nanostructure. *PLoS Biology*, *2*(11), e329.
567 https://doi.org/10.1371/journal.pbio.0020329

568 Dutta, S., Cruz, J. A., Imran, S. M., Chen, J., Kramer, D. M., & Osteryoung, K. W. (2017).
569 Variations in chloroplast movement and chlorophyll fluorescence among chloroplast division
570 mutants under light stress. *Journal of Experimental Botany*, *68*(13), 3541–3555.
571 https://doi.org/10.1093/jxb/erx203

572 Fujiwara, M. T., Yasuzawa, M., Kojo, K. H., Niwa, Y., Abe, T., Yoshida, S., Nakano, T., & Itoh,
573 R. D. (2018). The Arabidopsis arc5 and arc6 mutations differentially affect plastid morphology
574 in pavement and guard cells in the leaf epidermis. *PLOS ONE*, *13*(2), e0192380.
575 https://doi.org/10.1371/journal.pone.0192380

576 Fürtauer, L., Weckwerth, W., & Nägele, T. (2016). A Benchtop Fractionation Procedure for
577 Subcellular Analysis of the Plant Metabolome. *Frontiers in Plant Science*, *7*.
578 https://doi.org/10.3389/fpls.2016.01912

579 Fürtauer, L., Weiszmann, J., Weckwerth, W., & Nägele, T. (2018). Mathematical Modeling
580 Approaches in Plant Metabolomics. In C. António (Ed.), *Plant Metabolomics* (Vol. 1778, pp.
581 329–347). Springer New York. https://doi.org/10.1007/978-1-4939-7819-9_24

582 Goedhart, J., van Weeren, L., Hink, M. A., Vischer, N. O. E., Jalink, K., & Gadella, T. W. J.
583 (2010). Bright cyan fluorescent protein variants identified by fluorescence lifetime screening.
584 *Nature Methods*, *7*(2), 137–139. https://doi.org/10.1038/nmeth.1415

585 Harwood, R., Goodman, E., Gudmundsdottir, M., Huynh, M., Musulin, Q., Song, M., &
586 Barbour, M. M. (2020). Cell and chloroplast anatomical features are poorly estimated from 2D
587 cross-sections. *New Phytologist*, *225*(6), 2567–2578. https://doi.org/10.1111/nph.16219

588 Jarvis, P., & López-Juez, E. (2013). Biogenesis and homeostasis of chloroplasts and other
589 plastids. *Nature Reviews Molecular Cell Biology*, *14*(12), 787–802.
590 https://doi.org/10.1038/nrm3702

591 Johnson, D. E., Ai, H., Wong, P., Young, J. D., Campbell, R. E., & Casey, J. R. (2009). Red
592 Fluorescent Protein pH Biosensor to Detect Concentrative Nucleoside Transport. *Journal of*
593 *Biological Chemistry*, *284*(31), 20499–20511. https://doi.org/10.1074/jbc.M109.019042

Kinsman, E. A., & Pyke, K. A. (1998). Bundle sheath cells and cell-specific plastid development in *Arabidopsis* leaves. *Development*, *125*(10), 1815–1822. https://doi.org/10.1242/dev.125.10.1815

Kleine, T., Nägele, T., Neuhaus, H. E., Schmitz-Linneweber, C., Fernie, A. R., Geigenberger, P., Grimm, B., Kaufmann, K., Klipp, E., Meurer, J., Möhlmann, T., Mühlhaus, T., Naranjo, B., Nickelsen, J., Richter, A., Ruwe, H., Schroda, M., Schwenkert, S., Trentmann, O., … Leister, D. (2021). Acclimation in plants – the Green Hub consortium. *The Plant Journal*, *106*(1), 23–40. https://doi.org/10.1111/tpj.15144

Klie, S. (2011). Analysis of the compartmentalized metabolome – a validation of the non-aqueous fractionation technique. *Frontiers in Plant Science*, *2*. https://doi.org/10.3389/fpls.2011.00055

Koniger, M., Delamaide, J. A., Marlow, E. D., & Harris, G. C. (2008). Arabidopsis thaliana leaves with altered chloroplast numbers and chloroplast movement exhibit impaired adjustments to both low and high light. *Journal of Experimental Botany*, *59*(9), 2285–2297. https://doi.org/10.1093/jxb/ern099

Krantz, M., Zimmer, D., Adler, S. O., Kitashova, A., Klipp, E., Mühlhaus, T., & Nägele, T. (2021). Data Management and Modeling in Plant Biology. *Frontiers in Plant Science*, *12*, 717958. https://doi.org/10.3389/fpls.2021.717958

Kunz, H.-H., Gierth, M., Herdean, A., Satoh-Cruz, M., Kramer, D. M., Spetea, C., & Schroeder, J. I. (2014). Plastidial transporters KEA1, -2, and -3 are essential for chloroplast osmoregulation, integrity, and pH regulation in *Arabidopsis*. *Proceedings of the National Academy of Sciences*, *111*(20), 7480–7485. https://doi.org/10.1073/pnas.1323899111

616 Lampropoulos, A., Sutikovic, Z., Wenzl, C., Maegele, I., Lohmann, J. U., & Forner, J. (2013).
617 GreenGate—A Novel, Versatile, and Efficient Cloning System for Plant Transgenesis. *PLoS*
618 *ONE*, *8*(12), e83043. https://doi.org/10.1371/journal.pone.0083043

619 Liebers, M., Grübler, B., Chevalier, F., Lerbs-Mache, S., Merendino, L., Blanvillain, R., &
620 Pfannschmidt, T. (2017). Regulatory Shifts in Plastid Transcription Play a Key Role in
621 Morphological Conversions of Plastids during Plant Development. *Frontiers in Plant Science*,
622 *8*. https://doi.org/10.3389/fpls.2017.00023

623 Miyagishima, S., Froehlich, J. E., & Osteryoung, K. W. (2006). PDV1 and PDV2 Mediate
624 Recruitment of the Dynamin-Related Protein ARC5 to the Plastid Division Site. *The Plant Cell*,
625 *18*(10), 2517–2530. https://doi.org/10.1105/tpc.106.045484

626 Nobel, P. S. (2020). Water. In *Physicochemical and Environmental Plant Physiology* (pp. 53–
627 115). Elsevier. https://doi.org/10.1016/B978-0-12-819146-0.00002-X

628 Oi, T., Enomoto, S., Nakao, T., Arai, S., Yamane, K., & Taniguchi, M. (2017). Three-
629 dimensional intracellular structure of a whole rice mesophyll cell observed with FIB-SEM.
630 *Annals of Botany*, *120*(1), 21–28. https://doi.org/10.1093/aob/mcx036

631 Okazaki, K., Kabeya, Y., Suzuki, K., Mori, T., Ichikawa, T., Matsui, M., Nakanishi, H., &
632 Miyagishima, S. (2009). The PLASTID DIVISION1 and 2 Components of the Chloroplast
633 Division Machinery Determine the Rate of Chloroplast Division in Land Plant Cell
634 Differentiation. *The Plant Cell*, *21*(6), 1769–1780. https://doi.org/10.1105/tpc.109.067785

635 Osteryoung, K. W., & Pyke, K. A. (2014). Division and Dynamic Morphology of Plastids.
636 *Annual Review of Plant Biology*, *65*(1), 443–472. https://doi.org/10.1146/annurev-arplant-
637 050213-035748

638 Pipitone, R., Eicke, S., Pfister, B., Glauser, G., Falconet, D., Uwizeye, C., Pralon, T., Zeeman, S.
639 C., Kessler, F., & Demarsy, E. (2021). A multifaceted analysis reveals two distinct phases of
640 chloroplast biogenesis during de-etiolation in Arabidopsis. *ELife*, *10*, e62709.
641 https://doi.org/10.7554/eLife.62709

642 Pyke, K. A., & Leech, R. M. (1994). A Genetic Analysis of Chloroplast Division and Expansion
643 in Arabidopsis thaliana. *Plant Physiology*, *104*(1), 201–207.
644 https://doi.org/10.1104/pp.104.1.201

645 Robertson, E. J., Rutherford, S. M., & Leech, R. M. (1996). Characterization of Chloroplast
646 Division Using the Arabidopsis Mutant arc5. *Plant Physiology*, *112*(1), 149–159.
647 https://doi.org/10.1104/pp.112.1.149

648 Schulz, A., Knoetzel, J., Scheller, H. V., & Mant, A. (2004). Uptake of a Fluorescent Dye as a
649 Swift and Simple Indicator of Organelle Intactness: Import-competent Chloroplasts from Soil-
650 grown *Arabidopsis*. *Journal of Histochemistry & Cytochemistry*, *52*(5), 701–704.
651 https://doi.org/10.1177/002215540405200514

652 Sun, T., Yuan, H., Cao, H., Yazdani, M., Tadmor, Y., & Li, L. (2018). Carotenoid Metabolism in
653 Plants: The Role of Plastids. *Molecular Plant*, *11*(1), 58–74. https://doi.org/DOI:
654 10.1016/j.molp.2017.09.010

655 Unal, D., García-Caparrós, P., Kumar, V., & Dietz, K.-J. (2020). Chloroplast-associated
656 molecular patterns as concept for fine-tuned operational retrograde signalling. *Philosophical*
657 *Transactions of the Royal Society B: Biological Sciences*, *375*(1801), 20190443.
658 https://doi.org/10.1098/rstb.2019.0443

Waadt, R., Krebs, M., Kudla, J., & Schumacher, K. (2017). Multiparameter imaging of calcium and abscisic acid and high-resolution quantitative calcium measurements using R-GECO1-mTurquoise in Arabidopsis. *New Phytologist*, *216*(1), 303–320. https://doi.org/10.1111/nph.14706

Winter, H., Robinson, D. G., & Heldt, H. W. (1994). Subcellular volumes and metabolite concentrations in spinach leaves. *Planta*, *193*(4), 530–535. https://doi.org/10.1007/BF02411558

Woodward, A. W., & Bartel, B. (2018). Biology in Bloom: A Primer on the *Arabidopsis thaliana* Model System. *Genetics*, *208*(4), 1337–1349. https://doi.org/10.1534/genetics.118.300755

Yoshida, Y. (2018). Insights into the Mechanisms of Chloroplast Division. *International Journal of Molecular Sciences*, *19*(3), 733. https://doi.org/10.3390/ijms19030733

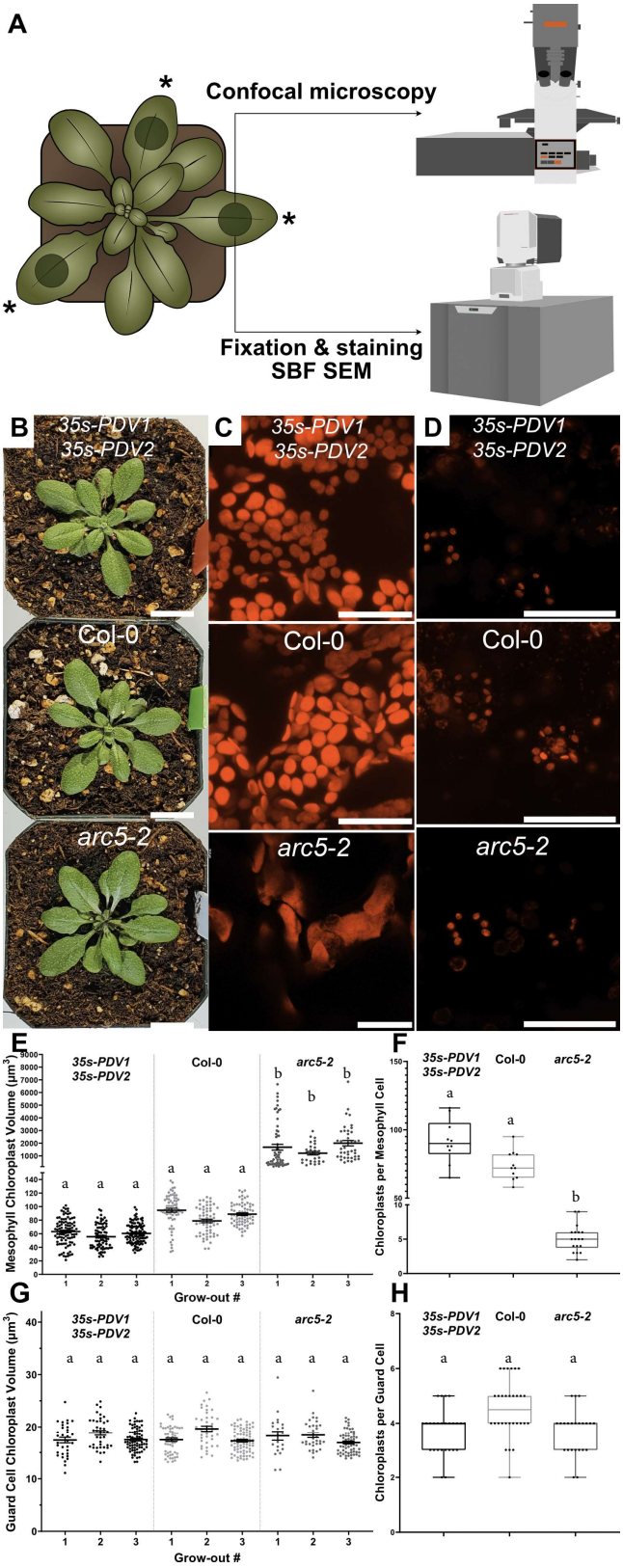
A
Confocal microscopy
Fixation & staining
SBF SEM
B
C
D
35s-PDV1
35s-PDV2
Col-0
arc5-2
E
F
G
H
Mesophyll Chloroplast Volume (µm³)
Chloroplasts per Mesophyll Cell
Guard Cell Chloroplast Volume (µm³)
Chloroplasts per Guard Cell
Grow-out #

Figure 1: Confocal microscopy reveals changes in gain and loss of function mutants in components of the plastid division machinery that are restricted to mesophyll cells. A, the diagram of the Arabidopsis plant shows the size of the plants when imaging and sample preparation was done. The * indicates the leaves used for imaging, and circles indicate the location on each leaf. From here, these samples were either used immediately for imaging using confocal microscopy or fixed and prepared for SBFSEM. **B**, No apparent changes in plant growth or appearance were observed in long-day cultivated genotypes used in this study, *35s-PDV1 35s-PDV2*, Col-0, *arc5-2* (scale bars = 2 cm). **C**, Confocal images of chlorophyll fluorescence for each genotype show clear size differences in mesophyll chloroplasts (scale bars = 25 µm). **D**, Confocal images of guard cell chloroplasts taken using chlorophyll fluorescence shows similar chloroplast volumes within guard cells of the three genotypes investigated (scale bars = 25 µm). **E**, Comparison of mesophyll chloroplast volumes deduced from z-stack of chlorophyll fluorescence recordings. Individual grow-outs are shown for each genotype. Statistical analysis done by one-way ANOVA with Tukey's multiple comparison test ($p<0.05$) showed no significant difference between Col-0 and *35s-PDV1 35s-PDV2* chloroplast volumes, neither in the full dataset, nor between any individual repetitions. Significant differences were observed between *arc5-2* and *35s-PDV1 35s-PDV2* but also between *arc5-2* and Col-0 mesophyll chloroplast volumes. Letters above each sample in the graph indicate groups of significance (±SE). **F**, Chloroplast numbers per mesophyll cell were counted and show an inverse relationship to that of chloroplast volumes observed between the genotypes. *35s-PDV1 35s-PDV2* has the highest average number of chloroplasts per cell with around 90 chloroplasts, followed by Col-0 averaging slightly fewer, at around 70 chloroplasts per cell. Finally, *arc5-2* mutants showed by far the lowest chloroplast count per cell with an average of 5 chloroplasts

(±SE). **G**, Guard cell chloroplast volumes calculated based on z-stacks of chlorophyll fluorescence recordings, in three separate grow outs, statistical analysis shows no significant difference ($p<0.05$) between any of the genotypes, neither within the whole dataset nor within individual growing cycles. Letters above each data set again show groups of significance (±SE). **H**, Guard cell chloroplast counts show that, unlike the similarities in volumes, a slight difference in average chloroplast number per guard cell can be observed. Col-0 guard cells contain on average 4.5 chloroplasts, while both the *35s-PDV1 35s-PDV2* and *arc5-2* genotypes contain only around 3.5 chloroplasts per guard cell (±SE).

672

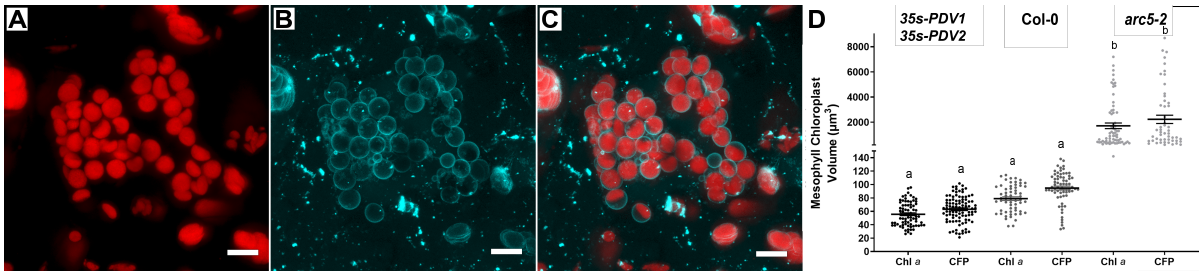

Figure 2: Comparing mesophyll chloroplast volumes deduced from chlorophyll fluorescence and an envelope membrane located fluorescent marker. Comparison of **A**, chlorophyll fluorescence, **B**, the outer chloroplast envelope labeled with CFP visualized in **C**, as an overlay in Col-0 (scale bar = 10 µm). **D**, comparison between chloroplast volumes extracted by chlorophyll fluorescence and mTurquoise envelope marker shows slightly higher volumes in each genotype when calculated using the mTurquoise marker. A statistically significant difference ($p<0.05$) in chloroplast volumes was only found between Col-0 and *35s-PDV1 35s-PDV2* when compared to *arc5-2* mutants. No significant difference is observed between imaging methods when looking at individual genotypes (±SE).

673

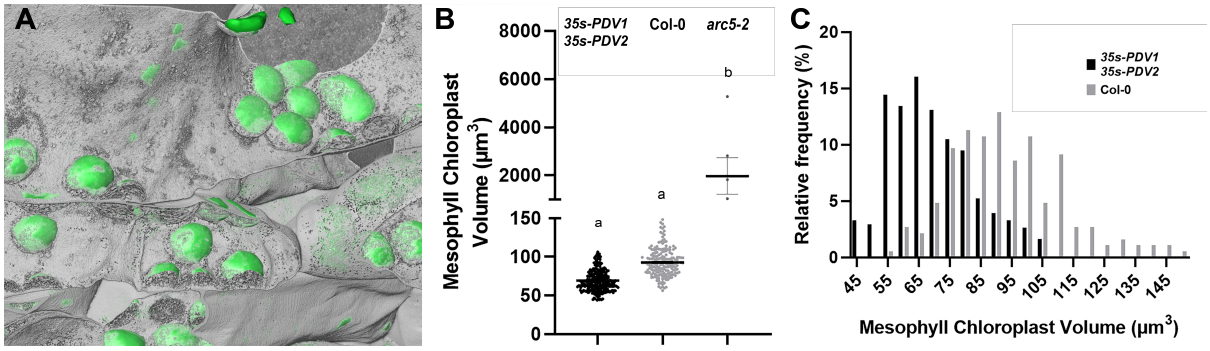

Figure 3: Chloroplast volume analysis using SBFSEM. A, Reconstructions of Col-0 chloroplasts by using SBFSEM. Green objects represent chloroplasts labeled using the machine learning algorithm, while in grey a surface was created by thresholding, representing mostly the cell wall and some other high contrast objects within the cells. **B**, deduced chloroplast volumes measured by SBFSEM imaging. Statistical significance ($p<0.05$) in chloroplast volumes is shown by numbers above each dataset in the graph. A significant difference in chloroplast volumes can only be seen between Col-0 and *arc5-2*, as well as between *35s-PDV1 35s-PDV2*, and *arc5-2*. **C**, A frequency distribution of Col-0 and *35s-PDV1 35s-PDV2* shows a shift in volume distribution between the two genotypes (±SE).

674

675

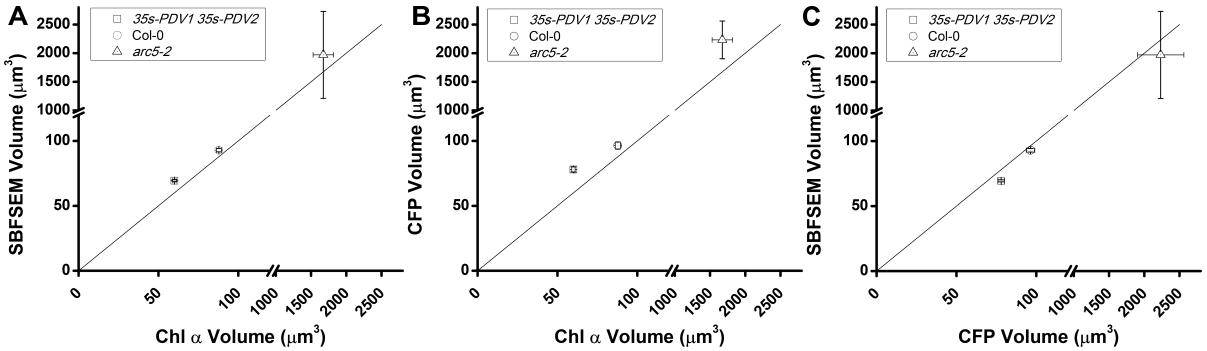

Figure 4: Comparison of chloroplast volumes measured by imaging type. A-C, comparison of mesophyll chloroplast volumes extracted using confocal imaging of chlorophyll fluorescence (Chl *a*), CFP envelope marker, and SBFSEM. The means of the data collected using each imaging method was taken for all genotypes. Each pair of imaging methods is compared by plotting the means (±SE). An identity line was added to highlight differences in means between imaging types in each graph. This shows overall similar volumes and distributions between the methods, with data extracted using the CFP envelope marker showing the largest volumes and chlorophyll fluorescence having the lowest. A one-way ANOVA done for statistical analysis only showing a significant difference ($p<0.05$) when comparing *35s-PDV1 35s-PDV2* and Col-0 volumes acquired by either method to *arc5-2*. No significant difference was found between imaging methods for any genotype.

676

677

678